ESTIMATE THE IMPACT OF DEEP EXCAVATION CONSTRUCTION IN HIGH-RISE BUILDINGS ON NEIGHBORING STRUCTURES

My PHAM*, Khanh-Toan LE

The University of Danang - University of Science and Technology, Vietnam

*Corresponding author: pmy@dut.udn.vn

(Received: April 14, 2024; Revised: May 28, 2024; Accepted: May 31, 2024)

Abstract - The estimation of diaphragm wall displacements and soil movement around the deep excavation of a high-rise building during the construction of basement floors plays a crucial role in limiting risks that may cause damages to human lives and property during the construction process. This study proposes the use of Finite Element Analysis (FEA) to accurately predict the behavior of soil and diaphragm walls in deep excavations of high-rise buildings. The model is based on advanced soil models and considers the interaction between diaphragm walls and soil, enabling the prediction of adverse impacts during the construction process, as well as negative effects on adjacent buildings. Additionally, the study will analyze and highlight the primary parameters that negatively impact the excavation process and neighboring constructions.

Key words - Bottom-up excavation; Top-down/Semi top-down excavation; Excavation Support System; Finite-element analysis; Hardening soil model; Ground movements.

1. Introduction

Due to limited urban space [1], high-rise buildings must integrate with underground space to address the increasing demand for parking lots, technical systems, and utilities for residential areas, as well as to increase stability for tall buildings. However, neighboring constructions near deep excavations may sustain damage due to the limited allowable settling difference during soil excavation [2, 3]. Because during the construction of a deep excavation, the soil's initial stress will be redistributed [4], resulting in deformation in both the diaphragm wall and the ground [5-7]. Therefore, when designing deep excavations, it is essential to evaluate and control the deformation of diaphragm walls and soil settling to ensure the safety of nearby structures [6-9]. In recent decades, the bottom-up [10-13] and top-down [14-17] methods have become common methods for constructing deep excavations (basements) in high-rise buildings. The majority of bottom-up methods utilize a bracing system or ground anchors to support the excavation walls, while top-down methods use the basement floors themselves as a bracing system for the excavation walls. Other special methods, such as the “central island technique” [18, 19] are also employed for wide and deep excavation conditions, among others. Therefore, evaluating the deformations of diaphragm walls and soil settling depend on the method used for constructing the basement/deep excavation of the high-rise building. There are two primary methods to predict soil movement and diaphragm wall displacement that may occur during soil excavation. The first method is based on experience. This method's advantage is that it makes it easy to reasonably and accurately predict soil settlement on projects with similar geological conditions, construction methods, and quality. For instance, Kung [20] describes an empirical radius model that can be acknowledged and verified through various records of completed quality projects. Additionally, this method provides a practical and straightforward design tool. Osman and Bolton [21, 22] proposed the Mobilizable Strength Design (MSD) method based on the deformation mechanism hypothesis between the structure and soil, rather than relying solely on the soil damage mechanism in which soil displacement is directly related to mobilized shear stress within the soil [23]. However, this method does not adequately describe the physical interaction between wall deflection and displaced surfaces, particularly in 3-D analysis [24]. The second method is the numerical approach, which generally includes the finite element method. Finite element analysis can accurately predict the deflection of diaphragm walls, but it often lacks accurate evaluation or prediction of ground surface settlement [25]. Therefore, this research trend has been expanded to many other related aspects. For example, FINNO [26] studied the three-dimensional impact caused by excavation at the corner of walls. Construction sequences can be efficiently simulated using a finite element model developed by FINNO [27, 28]. Furthermore, OU [29] analyzed the improvement of a certain underlying soil for excavation work using the finite element method.

However, very few studies have examined the interaction between diaphragm walls and the ground when using numerical methods to simulate the excavation process and predict the distribution of deformations of the diaphragm wall and the ground. NAKAI studied the sway of diaphragm walls without bracing systems with different surface roughness using the finite element method [24]. The combination of a flexible contact surface between the soil and the diaphragm wall was developed by NAKAI, and the numerical results were compared with experimental results. This showed that the friction between the diaphragm wall and the ground contributes to reducing the deformation of the wall and the displacement of the ground. This indicates that considering the analysis of friction on the diaphragm wall, the soil pressure acting on the diaphragm wall, and the displacement of the ground is crucial [30, 31]. However, further analysis of diaphragm walls with bracing systems presents difficulties and there are few reference materials available.

This study was conducted on a commercial center located on Ba Trieu Street in Hanoi, consisting of 27 above-ground floors and 3 basement levels constructed using the semi top-down method. The purpose of the study is to analyze the behavior of diaphragm walls in bracing systems for deep excavations using finite element analysis

while considering the interaction between the diaphragm wall and the ground in order to predict the displacement of the diaphragm wall and the movement of the soil, which may cause adverse effects on neighboring structures. A finite element model was created, and the contact surface between the diaphragm wall and the ground was modeled using the commercial software ABAQUS. The maximum sway amplitude and deformation of the diaphragm wall, as well as the movement of the ground, will be analyzed in multiple scenarios.

2. Description of construction site characteristics

The actual project is located on a plot of land with its front side adjacent to the existing VinCom building-1. One side of the project borders a residential area, while the other side is adjacent to Doan Tran Nghiep street. The back side of the project borders an empty plot of land. The specific location of the project is shown in the construction site plan in Figure 1.

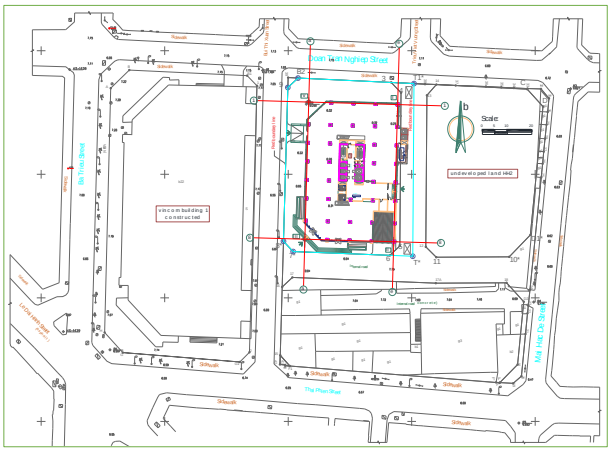

Figure 1. *Construction site layout and characteristics of the surrounding construction area of the project*

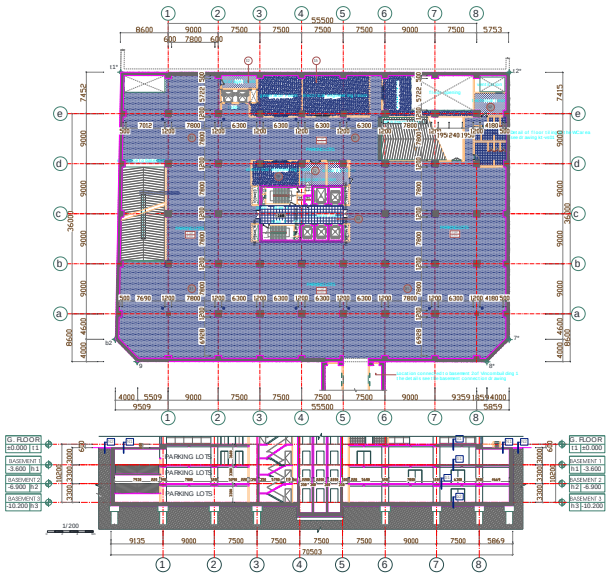

Figure 2. *Site plan, cross-section of the project basement*

The excavation pit has a natural ground level of -0.6m and a depth of -12.6m, resulting in a final depth of -13.2m (refer to Figure 2). The groundwater level is situated at a height of -2.5m. The pit has an area of 3,644.0m^2. Inclinometers have been installed around the excavation to monitor the displacement of the diaphragm wall as well as the soil's movement in both vertical and horizontal directions, ensuring safety throughout the excavation process.

3. Development of finite element analysis

With the development of multiple algorithms for computation analysis that offer high accuracy and reliability, FEA has become a popular tool for analyzing and designing deep excavations in both the design and construction stages of high-rise buildings. These findings have been supported by highly reliable and accurate field monitoring results [32-35]. Therefore, this study suggests that FEA is an effective approach for predicting and analyzing the impact on neighboring structures during the construction of deep excavations/basements in high-rise buildings. The soil material model used in this study is the Hardening Soil (HS) model, which is an advanced model capable of describing all working states of the excavation, such as compressive loading, deviatoric/shear loading, and unloading (see Figure 3). The FEA background was developed and applied to the specific problem of constructing deep excavations in high-rise buildings.

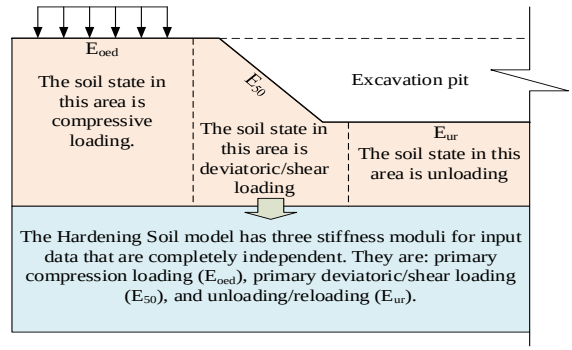

Figure 3. *Working diagram of the HS model in deep excavation*

3.1. Model and data of Soil

3.1.1. Hardening soil model

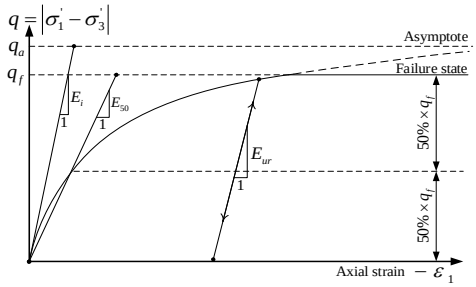

Figure 4. *Hyperbolic law for stress-strain relation in a standard drained triaxial test*

The idealized HS model represents the relationship between deviatoric stress (q) and vertical strain (ε_1) as a hyperbolic curve, as shown in Figure 4 (Duncan-Chang model [36]) during primary loading. Its yield curves are obtained from standard drained triaxial tests and can be described by equation (1) [37].

$$\varepsilon_1 = \frac{q_a}{2E_{50}} \frac{q}{q_a - q} \quad for \quad q < q_f \tag{1}$$

In which q_a represents the asymptotic value of the shear strength, calculated as $q_a = q_f / R_f$, where R_f is the failure

ratio, whose value ranges from 0.75 to 1 [36], with a typical standard value of 0.9 [38]. q_f refers to the ultimate deviatoric stress, obtained from the Mohr-Coulomb failure criterion, which is dependent on soil strength parameters such as c and φ. The expression for q_f is determined as follows:

$$q_f = \frac{6\sin\varphi}{3-\sin\varphi}\left(\sigma_3^{'} + c\cot\varphi\right) \quad (2)$$

In equation (1), E_{50} denotes the confining stress and serves as a substitute for the initial modulus (E_i) as a tangent modulus, especially in small strain applications where determining E_i through testing proves difficult. The reference stiffness modulus (E_{50}^{ref}) that corresponds to the reference stress (p^{ref}). It is used to determine E_{50}, as illustrated below:

$$E_{50} = E_{50}^{ref}\left(\frac{c\cos\varphi - \sigma_3^{'}\sin\varphi}{c\cos\varphi - p^{ref}\sin\varphi}\right)^m \quad (3)$$

In which σ_3' represents the minor principal stress and corresponds to the effective confining pressure in triaxial testing. m denotes the exponential stress-level dependency of stiffness. The value of m ranges from 0.5 to 1.0, with a value of 0.5 for sandy soil and a value of 1.0 for clay soil.

When the soil is in an unloading and reloading state, another stress-dependent stiffness modulus is used to describe the modulus of the soil as follows:

$$E_{ur} = E_{ur}^{ref}\left(\frac{c\cos\varphi - \sigma_3^{'}\sin\varphi}{c\cos\varphi - p^{ref}\sin\varphi}\right)^m \quad (4)$$

In which E_{ur}^{ref} represents the reference Young's modulus for both unloading and reloading states, corresponding to a reference pressure (p^{ref}).

In reality, the behavior of soil models is highly complex and dependent on the state of the soil at each point in time. Therefore, the HS model uses a stress-strain hyperbolic curve instead of the linear curve of the Mohr-Coulomb model, which is a significant improvement aimed at accurately simulating the soil's behavior. Additionally, the HS model enables the control of each stress level's stiffness modules. The elasto-plastic HS model cannot describe the relationship between the drained triaxial stiffness E_{50} and oedometer stiffness E_{oed}. Instead, these stiffnesses must be described independently of each other. The oedometer stiffness E_{oed} is a tangent stiffness modulus for primary loading, determined through a tangent stiffness at vertical stress $\sigma_1' = p^{ref}$, as shown in the equation.

$$E_{oed} = E_{oed}^{ref}\left(\frac{c\cos\varphi - \sigma_1^{'}\sin\varphi}{c\cos\varphi - p^{ref}\sin\varphi}\right)^m \quad (5)$$

3.1.2. Ground data

Developing a FEA model for the ground involves selecting ground dimensions (length, width, height) that are large enough to ensure that the diaphragm wall's impact does not affect the ground's outer boundary. Typically, the distance from the excavation's mouth to the ground's outer boundary should be no less than 1.5 to 2.0 times the excavation's width. In this project's study, the excavation has dimensions of 70.05m×52.02m×12.6m. Therefore, the simulated ground sizes have been chosen to be about 273.0m×202.0m×35.0m (shown in Figure 5). The ground used in the analysis model comprises four main layers in the following order of decreasing depth: Fill, Clay, Sand, and Deep sand. The geometrical and mechanical properties of the soil layers were obtained from geological drilling data conducted to meet the requirements of design and construction appropriate for the intended soil model used for analysis and calculation of construction methods for the excavation, as shown in Table 1.

Table 1. *Basic mechanical properties of the soil at the project construction area*

Parameter	Symbol	Fill	Clay	Sand	Deep sand	Unit
Material model	-	HS	HS	HS	HS	-
Drainage type	-	Drained	Undrained	Drained	Drained	-
Unit weight above phreatic level	γ_{unsat}	16	16	16.5	17	kN/m^3
Unit weight below phreatic level	γ_{sat}	20	17	20	21	kN/m^3
Secant stiffness for CD triaxial test	E_{50}^{ref}	$22\cdot10^3$	$2.0\cdot10^3$	$25\cdot10^3$	$42\cdot10^3$	kN/m^2
Tangent oedometer stiffness	E_{oed}^{ref}	$22\cdot10^3$	$2.0\cdot10^3$	$25\cdot10^3$	$42\cdot10^3$	kN/m^2
Unloading / reloading stiffness	E_{ur}^{ref}	$66\cdot10^3$	$10\cdot10^3$	$75\cdot10^3$	$126\cdot10^3$	kN/m^2
Power for stress-level dependency of stiffness	m	0.5	1	0.5	0.5	-
Cohesion	c_{ref}'	1	5	0	0	kN/m^2
Friction angle	φ'	30	25	31	35	°
Dilatancy angle	ψ	0	0	1	5	°
Poisson's ratio	ν_{ur}'	0.2	0.2	0.2	0.2	-
Strength reduction factor	R_i	0.65	0.5	1.0	0.7	-
Soil layer thickness	h	2	10.5	4.0	≥ 8.0	m

Table 2. *Basic mechanical properties of the soil Danang city*

Parameter	Symbol	Silt	Loam	Sand	Dense sand	Unit
Material model	-	HS	HS	HS	HS	-
Drainage type	-	Drained	Undrained	Drained	Drained	-
Unit weight above phreatic level	γ_{unsat}	16	17	17	20	kN/m^3
Unit weight below phreatic level	γ_{sat}	20	19	20	22	kN/m^3
Secant stiffness for CD triaxial test	E_{50}^{ref}	$20\cdot10^3$	$12\cdot10^3$	$30\cdot10^3$	$45\cdot10^3$	kN/m^2
Tangent oedometer stiffness	E_{oed}^{ref}	$20\cdot10^3$	$8.0\cdot10^3$	$30\cdot10^3$	$45\cdot10^3$	kN/m^2
Unloading / reloading stiffness	E_{ur}^{ref}	$60\cdot10^3$	$36\cdot10^3$	$90\cdot10^3$	$135\cdot10^3$	kN/m^2
Power for stress-level dependency of stiffness	m	0.5	0.8	0.5	0.5	-
Cohesion	c_{ref}'	1	5	0	5	kN/m^2
Friction angle	φ'	30	29	34	35	°
Dilatancy angle	ψ	0	0	4	0	°
Poisson's ratio	ν_{ur}'	0.2	0.2	0.2	0.2	-
Strength reduction factor	R_i	0.65	1.0	0.7	0.7	-
Soil layer thickness	h	3.0	12.0	6.0	≥ 10.0	m

Additionally, this study aims to investigate the behavior of the diaphragm wall and soil when there is a change in the mechanical properties of the soil. This analysis allows us to predict the level of impact that the project will have on the surrounding area by using the mechanical properties of the soil, as well as the size and structure of the excavation. Soil data from Danang was used for this study due to its better mechanical properties (refer to Table 2 for geological survey data), while the thickness of the soil layers is similar to that of the original soil where the project

is located (Hanoi city). The study conducted simulations and compared the results obtained using the Danang soil data with the results obtained using the original soil data. The soil data is provided in Table 2.

3.2. Governing equation and mesh generation for soil

Soil, covering much of the Earth's crust, is a complex system with solid, liquid, and gas phases. The solid phase comprises mineral particles of varying sizes occupying most of the soil's volume. The liquid phase, predominantly water with dissolved salts, fills the voids in the soil. Water greatly impacts the soil's mechanical properties, especially with smaller mineral particles and organic matter. The gas phase, mainly air, occupies the remaining voids and can be categorized into free gas and gas dissolved in water, each affecting the soil's properties differently [39, 40].

Since soil comprises three phases, understanding its mechanical properties involves considering the impact of both liquid and gas phases. In this study, the groundwater level distinguishes soil regions with active or passive pore pressures. Below this level, soil is fully saturated with positive pore pressure, while above it, the soil is unsaturated with negative pore pressure, influenced by surface tension and particle size. Fluctuations in pore water pressure alter shear strength, crucial for slope stability [41]. Therefore, the governing equation describing the behavior of the soil is a combination of the solid mechanics equation describing the soil skeleton and the fluid mechanics equation describing the liquid and gas in the soil's porous space. This equation was introduced in Pham's study [42], as follows:

$$\begin{bmatrix} \mathbf{K} & \mathbf{L} \\ \mathbf{L}^T & -\mathbf{S}^* \end{bmatrix} \begin{bmatrix} \Delta \boldsymbol{v} \\ \Delta \mathbf{p}_n \end{bmatrix} = \begin{bmatrix} 0 & 0 \\ 0 & \Delta t \mathbf{H}^* \end{bmatrix} \begin{bmatrix} \boldsymbol{v}_0 \\ \mathbf{p}_{n0} \end{bmatrix} + \begin{bmatrix} \Delta \mathbf{f}_n \\ \Delta t \mathbf{q}_n \end{bmatrix} \quad (6)$$

where $\boldsymbol{v}$ and $\boldsymbol{p}_n$ are the discrete nodal values of displacement and pore pressure, respectively; Δ is the finite difference operator; $\boldsymbol{K}$, $\boldsymbol{L}$, $\boldsymbol{f}$, $\boldsymbol{H}$, $\boldsymbol{S}$, $\boldsymbol{q}_n$, and Δt are the stiffness matrix, coupling matrix, incremental load vector, permeability matrix, compressibility matrix, prescribed recharges, and time stepping schema, respectively. All expressions are presented in Pham's study [42].

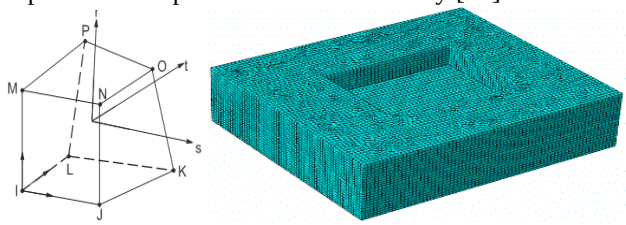

a) b)

Figure 5. *Generating the mesh for the soil: a) C3D8P element; b) Ground mesh in FEA*

The governing equation (6) describes the diffusion of the interacting liquid pressure with the mineral structure of the soil as a time-dependent process. Therefore, the 3D C3D8P element is used in this analysis, which is a fluid-porous/stress element with a cube shape and 8 Gauss integration points, with degrees of freedom at the nodes of the element being displacements in the x, y, z directions, and pore pressure. The element type used to generate the grid is shown in Figure 5-a, and the results of generating the grid for the soil are presented in Figure 5-b.

3.3. Finite element model of soil diaphragm walls

The perimeter of the diaphragm wall is a polygonal. Moreover, the project in this study was selected the semi top-down construction method. Consequently, it requires the use of reinforced concrete walls. In this study, the wall was 0.8 meters thick and 20.2 meters deep. The concrete material properties used in the diaphragm wall was based on experimental data from the study by Uwe S. [43]. After determining the geometry and material, the diaphragm wall was meshed using 8-node 3D-stress C3D8R elements, which are cubic elements with a reduced Gauss integration point technique to a single integration point. Moreover, due to the relatively large thickness of the reinforced concrete wall, the use of continuum elements is reasonable because these elements accurately describe the physical behavior in terms of the stress-strain relationship in the tension and compression regions of the wall with high precision. Furthermore, C3D8R elements are equipped with a reduced integration technique to tackle shear locking. The use of this element type provides a high accuracy in the stress-strain relationship at each integration point, with the integration point located at the element center. Thus, smaller element sizes are needed to accurately capture stress concentrations at the corner and boundary positions of the structure. The generated mesh is shown in Figure 6.

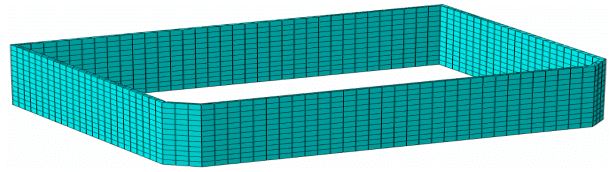

Figure 6. *Generating the mesh for the diaphragm wall*

3.4. Finite element model for the bracing system

The load-bearing and supporting system for the diaphragm wall in the semi top-down construction method includes the basement-level concrete floor, king-post, and shoring system at the floor openings. The 200mm-thick reinforced concrete floor and the basement were meshed using 8-node 3D-stress C3D8R elements as described in section 3.3. The remaining king-post H600×400×30 ×20 with a length of 14.6m, and shoring H400×300×20 ×10 at the construction opening are thin-walled steel structures. Hence, the S4R is a shell element recommended for meshing these structures. The S4R element can accurately describe the physical behavior (stress-strain) of these thin-walled structures. However, in thin-walled structures, two cases should be taken into account: First, reduced integration technique is applied. If the ratio of column/beam length to the cross-sectional dimension is quite large (for example, if the ratio of the column length/beam length to the cross-sectional dimension is larger than 40 times), the use of reduced integration technique can produce better results than using the full number of integration points. However, thin-walled sections are prone to hour-glassing, which results in inaccurate displacement fields. To overcome this, the average displacement of the cross-section is commonly used; Second, thin-walled structures are prone to large translation or rotation deformations. Therefore, in most cases, we need to use nonlinear geometric theory for

accurate results. The mesh generated for the shoring system of the soil barrier is shown in Figure 7.

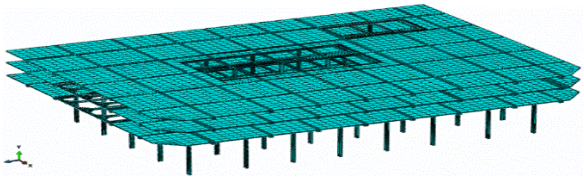

Figure 7. *Generating the mesh for the shoring system, including the kingpost and basement floor beams*

The mesh generated for the entire system, including the soil, the diaphragm wall, and its shoring-kingpost system, using the semi top-down construction method, is shown in Figure 8.

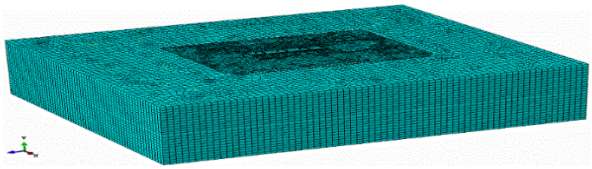

Figure 8. *Generating the mesh for the entire excavation system of the basement*

3.5. Interaction between the soil and the diaphragm wall

The interaction between the soil and the diaphragm wall is modeled using zero thickness interface elements [44] that can describe the physical nature of the interaction between the soil and the diaphragm wall, including wall friction, slip, and gapping between the soil and the structure. The interface material uses a strength reduction factor (SRF) (R_i) to describe the mechanical properties at the contact area between the soil and the diaphragm wall as shown in the following equation [45]:

$$\begin{cases} c_i = R_i c_{soil} \\ \varphi_i = \tan^{-1}\left(R_i \tan\varphi_{soil}\right) \\ G_i = R_i^2 G_{soil} = R_i^2\left[\dfrac{E_{soil}}{2\left(1+\nu_{soil}\right)}\right] \\ E_{oed,i} = 2G_i\dfrac{1-\nu_i}{1-2\nu_i} \\ E_i = 2G_i\left(1+\nu_i\right) = 1.45R_i^2\left[\dfrac{E_{soil}}{2\left(1+\nu_{soil}\right)}\right] \end{cases} \quad (7)$$

where c, φ, G, E and ν are soil cohesion, soil friction angle, shear modulus, Young's modulus, and Poisson's ratio, respectively; subscript "i" and "$soil$" represent the interface material and soil material; E_{oed} is the oedometer modulus. Note that in this study, the Poisson's ratio of the interface material is assumed to be $\nu_i = 0.45$. Depending on the type of soil and the material of the diaphragm wall structure, the corresponding SRF is proposed as shown in Table 3. Therefore, if using equation (7) and the data of the soil provided in Table 1, the mechanical properties of the interface material can be determined.

Table 3. *SRF by soil type and diaphragm wall structure type*

ID	Soil Type	Material Type	SRF (R_i)
1	Sand	Steel	0.6 ÷ 0.7
2	Clay	Steel	0.5
3	Sand	Concrete	0.8 ÷ 1.0
4	Clay	Concrete	0.7 ÷ 1.0
5	Soil	Geotextile	0.5 ÷ 0.9
6	Soil	Geogrid	1.0

4. Results and discussion

4.1. Behavior of soil

4.1.1. Pressure of the soil acting on the diaphragm wall

The pressure of the soil on the diaphragm wall is investigated, and in the study, active and passive soil pressures acting on the diaphragm wall are surveyed for two types of soil with different geology, as presented in section 3.1.2. The results shown in Figure 9 indicate that the active soil pressure acting on the diaphragm wall at a depth of approximately 8.0m initially increases linearly, and after exceeding 8.0m, it develops rapidly in a nonlinear rule. This result is due to the fact that the geological layers of both types of soil do not change significantly in the first 8.0m depth, while there are large variations in soil density, internal friction angle, and the impact of groundwater beyond 8.0m depth. On the other hand, the passive soil pressure due to the influence of active soil pressure gradually increases in a nonlinear rule. The results also indicate that in the good soil of Danang city, the active soil pressure on the diaphragm wall is lower than that in the weak soil found at the project site in Hanoi. Conversely, the passive soil pressure is higher. This difference can be attributed to the ability of the good soil in Danang city to resist higher pressure from the diaphragm wall, in contrast to the weaker soil present at the project location in Hanoi.

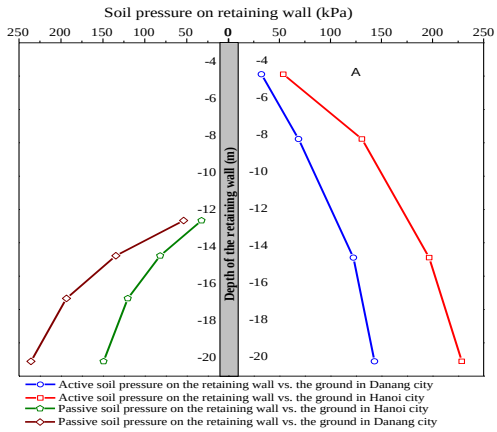

Figure 9. *Pressure of the soil acting on the diaphragm wall*

Figure 10 shows the law of the lateral pressure's impact on the lateral displacement of the diaphragm wall. The result is represented in a non-dimensional form (see Figure 10). When the diaphragm wall displaces out of the mouth of excavation pit (with a negative value), the diaphragm wall pressure increases significantly with relatively small displacement. However, when there is a relatively large displacement, the pressure on the diaphragm wall increases slowly. Because when the diaphragm wall displaces dramatically, it affects the soil, potentially causing soil structure damage. Consequently, the soil displacement in the direction of the wall displacement, resulting in a slow increase in pressure on the diaphragm wall, as described in Figure 10. On the other hand, when the diaphragm wall displaces into the excavation pit (with a positive value), the pressure of the soil on the diaphragm wall decreases. For dense sandy soil, the impact of the diaphragm wall's displacement on the soil pressure on the diaphragm wall increases/decreases, and the absolute value is larger than

that of the weak soil. Therefore, the interaction between the diaphragm wall and the soil reveals that the displacement of the diaphragm wall increases/decreases the pressure of the soil on the diaphragm wall, and depending on the different geological structures of the soil, the value of the pressure on the diaphragm wall also changes. This is also an important factor in calculating, designing, and selecting the diaphragm wall construction method.

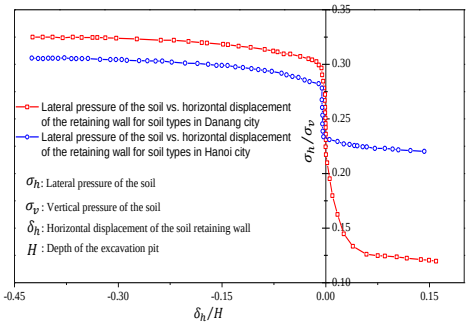

Figure 10. *Impact of lateral displacement on the pressure of soil acting on the diaphragm wall*

4.1.2. Stress in the soil

The distribution of the principal stress σ_{22} parallel to the natural ground surface and the shear stress τ in the soil help us determine whether the placement of the diaphragm wall is reasonable to ensure that the soil is not damaged, causing subsidence that affects the working conditions of the diaphragm wall and the construction site.

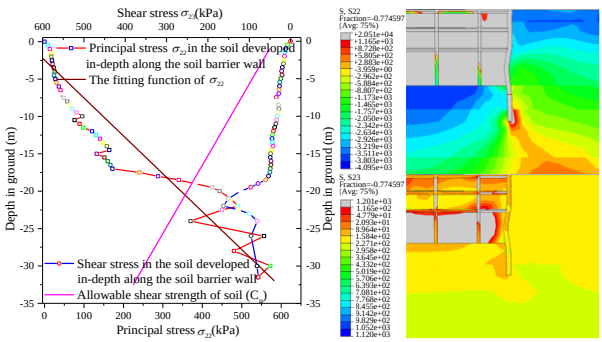

Figure 11. *Distribution of principal stresses σ_{22} and shear stress in the soil*

The results show that the principal stress σ_{22} and the shear stress τ are concentrated at the base of the diaphragm wall (see Figure 11). Therefore, calculating and selecting the soil layer to place the base of the diaphragm wall so that the allowable principal stress and shear stress of the soil layer at the base of the diaphragm wall must ensure that there is no occurrence of plastic deformation or sliding at the plane where the base of the diaphragm wall is placed. If the shear stress exceeds the permissible shear stress line C_u, the soil structure will be damaged. The permissible shear stress line C_u is determined from the results of soil surveys.

4.1.3. Lateral displacement of the soil

The lateral displacement of soil around excavation sites has significant importance in the design and construction of diaphragm walls. During the simulation process, we can predict the lateral displacements to assess their impact on neighboring structures, allowing designers to choose appropriate handling and construction measures to avoid accidents during construction.

The construction site has a rectangular ground plan with a beveled corner (see Figure 1), where we conducted to survey lateral displacements on all sides of the site. The surveyed sides are labeled as AB, CD, EF, and AF. The results show that the lateral displacement of the soil on the AF side is the largest, and the EF side is the smallest. The results accurately reflect the physical nature of the problem: the AF side has the longest length and is closest to the floor opening for transporting soil and construction equipment up and down with respect to the excavation pit, causing the largest lateral displacement for the AF side. The CD side has a shorter length than the AF side and has two beveled corners that enhance the corner effect compared to the right angle at the AF side. Moreover, it is far from the floor opening, resulting in smaller displacement than the AF side. The EF and AB sides have the same length and working conditions, but the AB side is closer to the floor opening, resulting in larger soil displacement than the EF side.

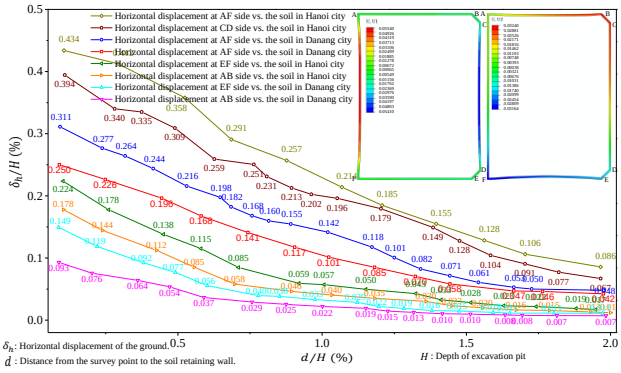

Figure 12. *Lateral displacement of the diaphragm wall during interaction with the soil*

In addition, the research results also compare the impact of different types of soil on their lateral displacement. For the same project, two different types of soil were surveyed with relatively different characteristics: one is weak soil in Hanoi city where the project is located, and the second soil, with geology chosen from Danang city, has a layer thickness that is not significantly different from the soil in Hanoi, but it has better physico-mechanical properties (see Table 1 and Table 2). The results show that the lateral displacement of ground in Danang city decreased by about 10.15%. This shows that for the same project placed in areas with different geological conditions, the degree of impact on lateral displacement of soil is also different, and this will provide us with different handling solutions. Therefore, the engineers who are responsible for designing the construction methods for deep excavations (basements) in high-rise buildings should pay attention to this aspect in order to propose reasonable and effective construction measures.

4.1.4. Settlement of the ground

Similar to lateral displacement, the settlement of the ground in the neighboring area of the diaphragm wall is an important factor that needs to be surveyed. The results in Figure 13 are completely similar to those in lateral displacement, meaning that the AF side has the largest settlement, and the EF side has the smallest settlement. From the survey results, it can also be seen that in all cases,

the settlement of the ground in the neighboring area of the diaphragm wall, and at a distance from the diaphragm wall of between (0.2-0.8) times the excavation depth, has the largest settlement. This result can also be explained by the fact that at the position where the soil contacts the diaphragm wall, the friction between the soil and the diaphragm wall prevents the ground from settling immediately at the contact position and instead causes the ground to settle at a distance from the wall of about 0.2H.

The results also indicate that the settlement of the ground is dependent on the soil type and the structure of the diaphragm wall. If the soil is weak and the diaphragm wall is not very rigid, the settlement of the soil will be relatively high. Using the simulation results, it is possible to predict the settlement of the ground, and subsequently predict the potential impact on neighboring structures. This knowledge can help in proposing appropriate and effective design and construction measures.

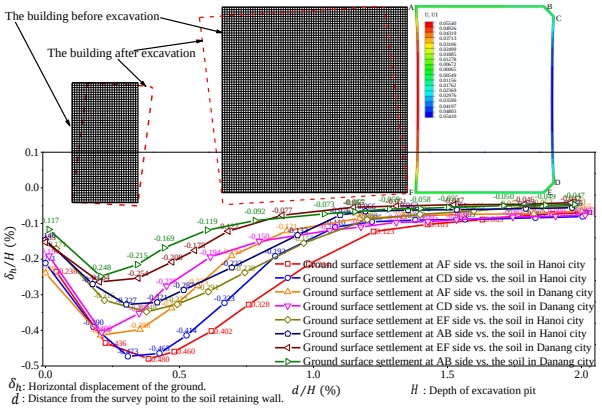

Figure 13. *Simulation results of the settlement of the soil outside the diaphragm wall*

Figure 14 depicts the settlement of the ground of the pedestrian way adjacent to the diaphragm wall of a deep excavation project in District 8, Ho Chi Minh City. The cause of the settlement of the soil is analyzed as the simulation results shown in Figure 13. The results demonstrate that failing to factor in the settlement of the ground around the excavation during the design of basement construction methods can result in a significant flaw. This can cause neighboring structures to tilt and settle, resulting in significant economic damages and safety hazards during the construction process, as illustrated in Figure 13 and Figure 14. This study illustrates that the utilization of calculation and simulation methods, as seen in Figure 13, enables the prediction of severe impacts on neighboring constructions beforehand, preventing catastrophic incidents that can lead to significant damage to nearby structures, as depicted in Figure 14.

Figure 14. *Settlement of the soil affects the neighboring structures of the actual construction project in District 8, Ho Chi Minh City*

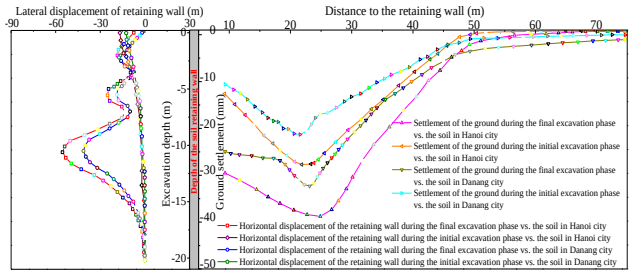

Figure 15. *Investigation of displacements between the diaphragm walls and the soil in Hanoi and Danang*

Figure 15 presents the results of the investigation into the interaction between the soil and the diaphragm wall. The results demonstrate a correlation between the displacement of the diaphragm wall and the settlement of the soil around the excavation. The study only compares this correlation during the initial excavation stage and the final stage (end of excavation process). In the initial stage, the displacement of the diaphragm wall is significant at the top of the wall, but in the final stage, the greatest displacement moves down to the bottom of the excavation pit and the corresponding settlement changes for each stage are described in Figure 15. These results will be analyzed in more detail in section 4.2.1.

4.2. Behavior of the diaphragm wall

4.2.1. Displacement

Figure 16 illustrates the horizontal displacement of the diaphragm wall for each excavation stage with geological data at the project location in Hanoi city. The bracing diagram in each construction stage is also described in Figure 16. Before excavating the basement floor, the diaphragm wall must be constructed with a cap-beam on top of it, at a height of 1.2m above natural ground level. In stage I, the excavation was carried out to a depth of -1.2m to install the formwork scaffolding system for the ground floor construction. In stage II, excavation was continued to a depth of -3.6m, and then the construction of the first basement floor was carried out. In stage III, the excavation was carried out to a depth of -7.2m, and then the second basement floor was constructed. In stage IV, excavation was carried out to a depth of -12.6m to construct the pile foundation, pile bracing, and the third basement floor, with the diaphragm wall base located at a depth of -20.2m.

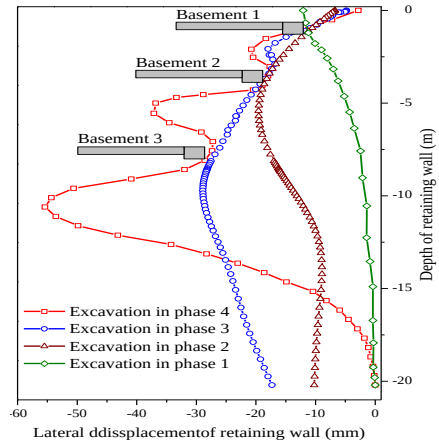

Figure 16. *The displacement of the diaphragm wall during the excavation phases*

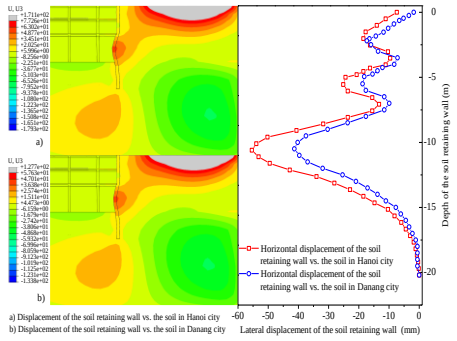

Figure 17. *Displacement of the diaphragm wall*

In phase 1, after lowering the ground level to the depth of -1.2m for the ground floor construction, the displacement of the diaphragm wall was approximately 12.1mm. At this point, the ground floor had not been constructed yet, so the diaphragm wall was acting as a cantilever diaphragm wall with one end pushed into the ground. In phase 2, after constructing the ground floor, the excavation continued to a depth of -3.6m to construct the first basement floor. At this stage, the diaphragm wall was cantilevering from the top, braced by the ground floor. The pressure applied on the diaphragm wall at this stage consisted not only of the construction loads but also of the active earth pressure from the natural ground surface to the basement floor level. This resulted in a displacement of 17.5mm at the basement floor level. Similarly, the displacement increased gradually due to the increased active earth pressure on the diaphragm wall at the levels of the second basement floor and the excavation bottom (foundation pit bottom). The displacement reached maximum at the midpoint between each basement floor level and achieved its peak at the bottom of the excavation (55.4mm). The increasing value of displacement was due to the increased active earth pressure acting on the diaphragm wall, while the sudden increase in displacement at the bottom of the excavation was because of the greater distance of the bracing system from the diaphragm wall at this stage, resulting from the excavation process and the lowered ground level to the base of the foundation.

In this study, we also compared this correlation between two types of soil: one representing good soil in Danang city (the soil parameters provided in Table 2) and the other representing weaker soil at the construction site in Hanoi city (the soil parameters provided in Table 1). The results showed that the soil in Danang city resulted in significantly smaller displacement of the diaphragm wall and less soil settlement compared to the soil in Hanoi city. This indicates that the construction site location plays a crucial role in designing construction measures for deep excavation in high-rise buildings.

4.2.2. Internal forces in the diaphragm wall

Firstly, the vertical force in the diaphragm wall is analyzed. The vertical force in the diaphragm wall increases gradually and attains its maximum value at the bottom of the excavation (-214.11kN/m) before decreasing towards the bottom of the diaphragm wall (refer to Figure 18-a). The distribution rule of the vertical force is consistent with the physical nature of the interaction between the soil and the diaphragm wall. The cause of the vertical force in the diaphragm wall is due to the self-weight of the diaphragm wall and partly due to the load transmitted from the ground floor and basement floors. These forces are balanced with the frictional force between the diaphragm wall and the soil from the start of the diaphragm wall to the bottom of the diaphragm wall. As the frictional force between the diaphragm wall and the soil increases from the bottom of the basement floor to the bottom of the diaphragm wall, the vertical force in the diaphragm wall decreases correspondingly and ultimately becomes negligible at the bottom of the diaphragm wall.

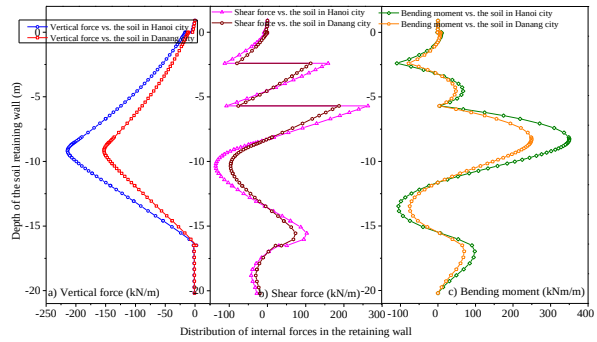

Figure 18. *Distribution of internal force in the diaphragm wall*

Shear force is one of the crucial parameters in calculating and designing diaphragm wall construction measures. Investigating the distribution law of the shear force in the diaphragm wall and the diaphragm wall bracing system is essential. In this study, through the analysis and calculation process, we obtained the distribution law results of the shear force in Figure 18-b. The results of the analysis showed that the shear force reached its maximum value at the diaphragm wall bracing locations and gradually increased to its highest value at the third bracing level and the bottom of the excavation. This value was approximately 135.58kN/m, after which the shear force decreased slowly in the section where the diaphragm wall embedded in the soil. The obtained results showed a reasonable distribution of the shear force in the working diagram and calculation of the diaphragm wall. The concentrated shear force at the bracing system is due to the reaction force of the bracing system acting on the diaphragm wall, which increases at greater depths. It is because the active soil pressure acting on the diaphragm wall at these depths is greater, resulting in a more substantial load.

Figure 18-c illustrates the behavior law of the bending moment in the diaphragm wall. The bending moment reaches its maximum value at the point where the diaphragm wall embeds into the basement floor, the location between the two basement floors' spans, and where the soil changes from one layer to another when the diaphragm wall fully embeds into the soil. The maximum bending moment is reached at the bottom of the excavation, with a value of approximately 349.53kNm/m.

The internal forces in the diaphragm wall are also investigated between the weak soil (at the location of the project in Hanoi) and the good soil (taken in Danang). The results showed that the weak soil would cause greater internal forces than the good soil. Specifically, in this study, the internal force in the diaphragm wall for the weak soil in Hanoi increased by about 28.7% compared to the good soil in Danang.

4.3. Behavior of the bracing system

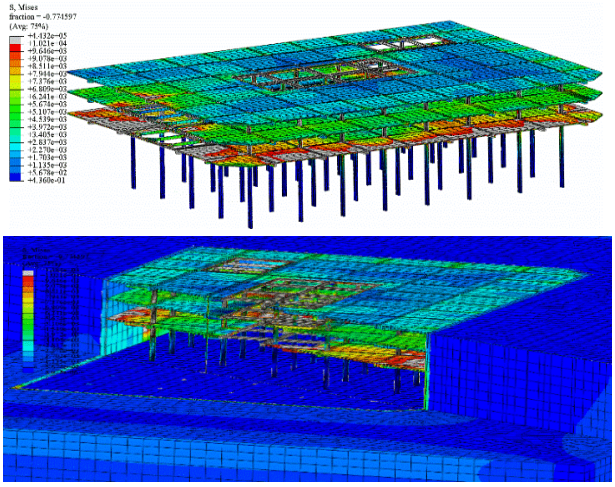

Figure 19. *Stress distribution in the bracing system*

Figure 19 illustrates the stress distribution in the bracing system constructed using the semi-top-down method to support the diaphragm wall. According to the simulation results presented in Figure 19, the highest stress in the bracing system is mainly concentrated on the second basement floor, with a value of 0.443 MPa. This stress is less than the compressive strength of the B30 concrete of the second-floor beam, which is 17 MPa, indicating that the bracing structure can withstand the pressure from the diaphragm wall. It is noteworthy that this maximum stress is mainly concentrated at the corner positions of the floor, the edge of the floor connecting to the soil diaphragm wall, and at the openings in the floor. Therefore, during the design and construction process, it is necessary to reinforce the steel bars at these critical locations.

5. Conclusion

Through the process of investigating the interaction between soil and diaphragm walls using a contact model to construct calculation models based on finite element analysis, some conclusions have been drawn:

- The displacement of the diaphragm wall gradually develops towards the bottom of the excavation. Specifically, the displacement of the diaphragm wall accumulates through each stage of excavation. Therefore, when simulating the excavation process, it must be carried out in the construction phases that reflect the actual situation on-site.
- Under weak geological conditions (where the values of elastic modulus (E), shear strength (c), and friction angle (φ) are low, as observed in the geological conditions in Hanoi where the project is located), the diaphragm wall experiences large displacements and low stress. Conversely, under good geological conditions (where the values of elastic modulus (E), shear strength (c), and friction angle (φ) are high, as observed in the geological conditions in Danang), the diaphragm wall experiences small displacements and high stress.
- The stiffness of the bracing system is relatively large for the first-floor basement and subsequent basement floors, and the connection between the diaphragm wall and the bracing system is a frictional connection. There is a distribution of internal forces in space, so the displacement and stress on the diaphragm wall are small.
- From the investigation of the interaction between soil and diaphragm walls using a contact model to construct calculation models based on the finite element method, we can determine the stress, horizontal displacement of the diaphragm wall, the settlement of the diaphragm wall and the surrounding soil. Therefore, the proposed construction measures can be used to minimize the settlement of adjacent structures.
- Stability analysis of the diaphragm walls can be conducted for each construction method, geological structure, and physical properties of the soil.
- An optimal solution for the construction of diaphragm walls in deep excavations can be proposed based on the corresponding geological structure and physical properties of the soil in different regions.

REFERENCES

[1] M. Dong and P. Jia, "Stability Analysis and Parameter Optimization of Deep Excavation Supporting System in Granular Soils", *Advances in Civil Engineering*, vol. 2020, p. 8873655, 2020, doi: https://doi.org/10.1155/2020/8873655.

[2] J. Finno Richard, T. Voss Frank, E. Rossow, and J. T. Blackburn, "Evaluating Damage Potential in Buildings Affected by Excavations", *Journal of Geotechnical and Geoenvironmental Engineering*, vol. 131, no. 10, pp. 1199-1210, 2005, doi: https://doi.org/10.1061/(ASCE)1090-0241(2005)131:10(1199).

[3] P. Guo, X. Gong, and Y. Wang, "Displacement and force analyses of braced structure of deep excavation considering unsymmetrical surcharge effect", *Computers and Geotechnics*, vol. 113, p. 103122, 2019, doi: https://doi.org/10.1016/j.compgeo.2019.103102.

[4] H. G. Poulos, "Analysis of Foundation Settlement Interaction among Multiple High-Rise Buildings", *Geotechnical and Geological Engineering*, vol. 41, no. 5, pp. 2815-2831, 2023, doi: https://doi.org/10.1007/s10706-023-02429-1.

[5] J. H. Wang, Z. H. Xu, and W. D. Wang, "Wall and Ground Movements due to Deep Excavations in Shanghai Soft Soils", *Journal of Geotechnical and Geoenvironmental Engineering*, vol. 136, no. 7, pp. 985-994, 2010, doi: https://doi.org/10.1061/(ASCE)GT.1943-5606.0000299.

[6] L. Wang, Z. Luo, J. Xiao, and C. H. Juang, "Probabilistic Inverse Analysis of Excavation-Induced Wall and Ground Responses for Assessing Damage Potential of Adjacent Buildings", *Geotechnical and Geological Engineering*, vol. 32, no. 2, pp. 273-285, 2014, doi: https://doi.org/10.1007/s10706-013-9709-4.

[7] Q. T. Huynh, V. Q. Lai, T. Boonyatee, and S. Keawsawasvong, "Behavior of a Deep Excavation and Damages on Adjacent Buildings: a Case Study in Vietnam", *Transportation Infrastructure Geotechnology*, vol. 8, no. 3, pp. 361-389, 2021, doi: https://doi.org/10.1007/s40515-020-00142-7.

[8] W. Pawirodikromo, "Ground Motions, Site Amplification and Building Damage at Near Source of the 2006 Yogyakarta, Indonesia Earthquake", *Geotechnical and Geological Engineering*, vol. 40, no. 12, pp. 5781-5798, 2022, doi: https://doi.org/10.1007/s10706-022-02249-9.

[9] J. J. Nisha, M. Muttharam, M. Vinoth, and C. R. E. Prasad, "Design, Construction and Uncertainties of a Deep Excavation Adjacent to the High-Rise Building", *Indian Geotechnical Journal*, vol. 49, no. 5, pp. 580-594, 2019, doi: https://doi.org/10.1007/s40098-019-00368-4.

[10] J. F. Richard, K. A. Dimitrios, and B. P. Scott, "Observed Performance of a Deep Excavation in Clay", *Journal of Geotechnical Engineering*, vol. 115, no. 8, pp. 1045-1064, 1989, doi: https://doi.org/10.1061/(ASCE)0733-9410(1989)115:8(1045).

[11] J. T. Blackburn and J. F. Richard, "Three-Dimensional Responses Observed in an Internally Braced Excavation in Soft Clay", *Journal of Geotechnical and Geoenvironmental Engineering*, vol. 133, no. 11, pp. 1364-1373, 2007, doi: https://doi.org/10.1061/(ASCE)1090-0241(2007)133:11(1364).

[12] M. A. H. Youssef, A. Osouli, and C. Marulanda, "Central Artery/Tunnel Project Excavation Induced Ground Deformations",

Journal of Geotechnical and Geoenvironmental Engineering, vol. 134, no. 9, pp. 1399-1406, 2008, doi: https://doi.org/10.1061/(ASCE)1090-0241(2008)134:9(1399).

[13] Y. Tan and B. Wei, "Observed Behaviors of a Long and Deep Excavation Constructed by Cut-and-Cover Technique in Shanghai Soft Clay", *Journal of Geotechnical and Geoenvironmental Engineering*, vol. 138, no. 1, pp. 69-88, 2012, doi: https://doi.org/10.1061/(ASCE)GT.1943-5606.0000553.

[14] J. Whittle Andrew, M. A. H. Youssef, and V. W. Robert, "Analysis of Deep Excavation in Boston", *Journal of Geotechnical Engineering*, vol. 119, no. 1, pp. 69-90, 1993, doi: https://doi.org/10.1061/(ASCE)0733-9410(1993)119:1(69).

[15] C.-Y. Ou, J.-T. Liao, and H.-D. Lin, "Performance of Diaphragm Wall Constructed Using Top-Down Method", *Journal of Geotechnical and Geoenvironmental Engineering*, vol. 124, no. 9, pp. 798-808, 1998, doi: https://doi.org/10.1061/(ASCE)1090-0241(1998)124:9(798).

[16] G. B. Liu, W. Ng Charles, and Z. W. Wang, "Observed Performance of a Deep Multistrutted Excavation in Shanghai Soft Clays", *Journal of Geotechnical and Geoenvironmental Engineering*, vol. 131, no. 8, pp. 1004-1013, 2005, doi: https://doi.org/10.1061/(ASCE)1090-0241(2005)131:8(1004).

[17] Y. Tan and M. Li, "Measured performance of a 26 m deep top-down excavation in downtown Shanghai", *Canadian Geotechnical Journal*, vol. 48, no. 5, pp. 704-719, 2011, doi: https://doi.org/10.1139/t10-100.

[18] Y. Tan and D. Wang, "Characteristics of a Large-Scale Deep Foundation Pit Excavated by the Central-Island Technique in Shanghai Soft Clay. I: Bottom-Up Construction of the Central Cylindrical Shaft", *Journal of Geotechnical and Geoenvironmental Engineering*, vol. 139, no. 11, pp. 1875-1893, 2013, doi: https://doi.org/10.1061/(ASCE)GT.1943-5606.0000928.

[19] Y. Tan and D. Wang, "Characteristics of a Large-Scale Deep Foundation Pit Excavated by the Central-Island Technique in Shanghai Soft Clay. II: Top-Down Construction of the Peripheral Rectangular Pit", *Journal of Geotechnical and Geoenvironmental Engineering*, vol. 139, no. 11, pp. 1894-1910, 2013, doi: https://doi.org/10.1061/(ASCE)GT.1943-5606.0000929.

[20] T. K. Gordon, C. H. Juang, C. H. Evan, and M. H. Youssef, "Simplified Model for Wall Deflection and Ground-Surface Settlement Caused by Braced Excavation in Clays", *Journal of Geotechnical and Geoenvironmental Engineering*, vol. 133, no. 6, pp. 731-747, 2007, doi: https://doi.org/10.1061/(ASCE)1090-0241(2007)133:6(731).

[21] A. S. Osman and M. D. Bolton, "A new design method for retaining walls in clay", *Canadian Geotechnical Journal*, vol. 41, no. 3, pp. 451-466, 2004, doi: https://doi.org/10.1139/t04-003.

[22] A. S. Osman and M. D. Bolton, "Ground Movement Predictions for Braced Excavations in Undrained Clay", *Journal of Geotechnical and Geoenvironmental Engineering*, vol. 132, no. 4, pp. 465-477, 2006, doi: https://doi.org/10.1061/(ASCE)1090-0241(2006)132:4(465).

[23] P. J. Vardanega and M. D. Bolton, "Design of Geostructural Systems", *ASCE-ASME Journal of Risk and Uncertainty in Engineering Systems, Part A: Civil Engineering*, vol. 2, no. 1, p. 04015017, 2016, doi: https://doi.org/10.1061/AJRUA6.0000849.

[24] T. Nakai, H. Kawano, K. Murata, M. Banno, and T. Hashimoto, "Model Tests and Numerical Simulation of Braced Excavation in Sandy Ground: Influences of Construction History, Wall Friction, Wall Stiffness, Strut Position and Strut Stiffness", *Soils and Foundations*, vol. 39, no. 3, pp. 1-12, 1999, doi: https://doi.org/10.3208/sandf.39.3_1.

[25] G. T.-C. Kung, C.-Y. Ou, and C. H. Juang, "Modeling small-strain behavior of Taipei clays for finite element analysis of braced excavations", *Computers and Geotechnics*, vol. 36, no. 1, pp. 304-319, 2009, doi: https://doi.org/10.1016/j.compgeo.2008.01.007.

[26] J. F. Richard, J. T. Blackburn, and F. R. Jill, "Three-Dimensional Effects for Supported Excavations in Clay", *Journal of Geotechnical and Geoenvironmental Engineering*, vol. 133, no. 1, pp. 30-36, 2007, doi: https://doi.org/10.1061/(ASCE)1090-0241(2007)133:1(30).

[27] R. J. Finno and J. T. Blackburn, "Three-Dimensional Modeling of Excavation Sequences", in *GeoCongress 2006: Geotechnical Engineering in the Information Technology Age*, Atlanta, Georgia, United States, D. J. DeGroot, J. T. DeJong, D. Frost, and L. G. Baise, Eds., 2006: American Society of Civil Engineers, doi: https://doi.org/10.1061/40803(187)189.

[28] C. W. W. Ng and R. W. M. Yan, "Three-dimensional modelling of a diaphragm wall construction sequence", *Géotechnique*, vol. 49, no. 6, pp. 825-834, 1999, doi: https://doi.org/10.1680/geot.1999.49.6.825.

[29] C.-Y. Ou, F.-C. Teng, and I. W. Wang, "Analysis and design of partial ground improvement in deep excavations", *Computers and Geotechnics*, vol. 35, no. 4, pp. 576-584, 2008, doi: https://doi.org/10.1016/j.compgeo.2007.09.005.

[30] N. Benmebarek, S. Benmebarek, R. Kastner, and A.-H. Soubra, "Passive and active earth pressures in the presence of groundwater flow", *Géotechnique*, vol. 56, no. 3, pp. 149-158, 2006, doi: https://doi.org/10.1680/geot.2006.56.3.149.

[31] A. V. D. Bica and C. R. I. Clayton, "An experimental study of the behaviour of embedded lengths of cantilever walls", *Géotechnique*, vol. 48, no. 6, pp. 731-745, 1998, doi: https://doi.org/10.1680/geot.1998.48.6.731.

[32] T. Bhatkar, D. Barman, A. Mandal, and A. Usmani, "Prediction of behaviour of a deep excavation in soft soil: a case study", *International Journal of Geotechnical Engineering*, vol. 11, no. 1, pp. 10-19, 2017, doi: https://doi.org/10.1080/19386362.2016.1177309.

[33] H. Popa, A. Ene, R. Miritoiu, I. Ionescu, and D. Marcu, "Back analysis of an embedded retaining wall for a deep excavation in Bucharest", *ce/papers*, vol. 2, no. 2-3, pp. 743-748, 2018, doi: https://doi.org/10.1002/cepa.759.

[34] J. Chai, J. Ni, W. Ding, Y. Qiao, and X. Lu, "Deep excavation in under-consolidated clayey deposit", *Underground Space*, vol. 6, no. 4, pp. 455-468, 2021, doi: https://doi.org/10.1016/j.undsp.2020.08.001.

[35] M. Ünver and İ. S. Ünver, "Monitoring of a Deep Excavation Supported by Anchored Retaining Walls", *Indian Geotechnical Journal*, vol. 52, no. 1, pp. 227-236, 2022, doi: https://doi.org/10.1007/s40098-021-00544-5.

[36] M. D. James and C.-Y. Chang, "Nonlinear Analysis of Stress and Strain in Soils", *Journal of the Soil Mechanics and Foundations Division*, vol. 96, no. 5, pp. 1629-1653, 1970, doi: https://doi.org/10.1061/JSFEAQ.0001458.

[37] R. Kondner, "A hyperbolic stress-strain formulation for sands", in *Proc. second Pan-American Conf. on Soil Mech. and Found. Eng.*, 1963, vol. 1, pp. 289-324.

[38] P. A. Vermeer, "The hardening soil model: Formulation and verification", in *Beyond 2000 in computational geotechnics*, R. B. J. Brinkgreve Ed. A.A.Balkema, P.O.Box 1675,3000 BR Rotterdam, Netherlands: Taylor & Francis Group - Routledge, 1999, pp. 281-296.

[39] P. P. Raj, *Soil Mechanics and Foundation Engineering* (Always Learning). Dorling Kindersley, 2013.

[40] L. D. Wesley, *Fundamentals of Soil Mechanics for Sedimentary and Residual Soils*. Wiley, 2009.

[41] P. N. Modi, *Soil Mechanics and Foundation Engineering* (Soil Mechanics and Foundation Engineering). Amit Publisher and Distributors, 2017.

[42] P. My and L. Khanh-Toan, "Investigated Behavior of the Top-base Foundation Using Finite Element Analysis", *The University of Danang - Journal of Science and Technology*, vol. 20, no. 6, pp. 12-18, 2022, doi: https://doi.org/10.31130/ud-jst.2022.229E.

[43] U. Starossek, N. Falah, and T. Lohning, "Numerical analyses of the force transfer in concrete-filled steel tube columns", *Structural Engineering and Mechanics*, vol. 35, no. 2, pp. 241-256, 2010, doi: https://doi.org/10.12989/sem.2010.35.2.241.

[44] B. Cerfontaine, A. C. Dieudonné, J. P. Radu, F. Collin, and R. Charlier, "3D zero-thickness coupled interface finite element: Formulation and application", *Computers and Geotechnics*, vol. 69, pp. 124-140, 2015, doi: https://doi.org/10.1016/j.compgeo.2015.04.016.

[45] I. P. Damians, Y. Yu, A. Lloret, R. J. Bathurst, and A. Josa, "Equivalent interface properties to model soil-facing interactions with zero-thickness and continuum element methodologies", in *From Fundamentals to Applications in Geotechnics*: IOS Press, 2015, pp. 1065-1072.